ENVIRONMENTAL RESEARCH
LETTERS

LETTER • OPEN ACCESS

Representation of low-tropospheric temperature inversions in ECMWF reanalyses over Europe

Environmental Research Letters

LETTER

Representation of low-tropospheric temperature inversions in ECMWF reanalyses over Europe

Angelika Palarz[1], **Jürg Luterbacher**[2,3], **Zbigniew Ustrnul**[1], **Elena Xoplaki**[2] **and Daniel Celiński-Mysław**[1]

[1] Department of Climatology, Jagiellonian University in Krakow, Kraków, Poland
[2] Department of Geography, Climatology, Climate Dynamics and Climate Change & Center of International Development and Environmental Research, Justus Liebig University Giessen, Giessen, Germany
[3] Science and Innovation Department, World Meteorological Organization (WMO), Geneva, Switzerland

E-mail: angelika.palarz@doctoral.uj.edu.pl, jluterbacher@wmo.int, zbigniew.ustrnul@uj.edu.pl, elena.xoplaki@geogr.uni-giessen.de and daniel.celinski-myslaw@doctoral.uj.edu.pl

OPEN ACCESS

RECEIVED
28 November 2019

REVISED
25 February 2020

ACCEPTED FOR PUBLICATION
6 March 2020

PUBLISHED
6 July 2020

Keywords: temperature inversions, lower-tropospheric stability, ECMWF reanalyses, upper-air soundings, data evaluation

Abstract

Despite the fact that tropospheric temperature inversions are thought to be an important feature of climate as well as a significant factor affecting air quality, low-level cloud formation, and the radiation budget of the Earth, a quantitative assessment of their representation in atmospheric reanalyses is yet missing. Here, we provide new evidence of the occurrence of low-tropospheric temperature inversions and associated uncertainties in their parameters existing among reanalyses produced by the European Centre for Medium-Range Weather Forecasts (ECMWF) and upper-air soundings for Europe covering the period 2001–2010. The reanalyses utilized here include (1) surface-input reanalyses represented by ERA-20C and CERA-20C as well as (2) full-input reanalyses represented by ERA-Interim and ERA5. The upper-air soundings were derived from the Integrated Global Radiosonde Archive (IGRA), version 2. The data consists mainly of air temperature and geopotential height from the model levels (ModLev) and pressure levels (PresLev) of ECMWF reanalyses. The results show that the frequency of surface-based inversions (SBI) and elevated inversions (EI) is largely in agreement among the reanalyses. The quality of their representation depends, however, on the inversion type, season, and region. Over the vast majority of IGRA upper-air stations, SBI frequency is overestimated and EI frequency is underestimated by ECMWF reanalyses. Substantially larger uncertainties arise from the selection between the data of ModLev and PresLev of the reanalyses—the differences in the frequency of the temperature inversions are particularly large for summertime SBI suggesting that PresLev are not capable of resolving the main features of shallow and weak SBI.

1. Introduction

Atmospheric reanalyses, which are spatially and temporally coherent datasets providing a synthesized estimate of the past and current state of the Earth's atmosphere, have recently become widely used both in climate and environmental research as well as outside scientific applications (Gregow *et al* 2016, Hersbach *et al* 2018). They consist of diverse assimilation schemes, input observations, and numerical models, which may generate some uncertainties among various reanalysis types. According to Fujiwara *et al* (2017), the reanlayses may be grouped into two main categories: (1) surface-input reanalyses assimilating only surface observations and (2) full-input reanalyses assimilating also data from other sources, such as satellite and upper air soundings. The latter are thought to offer a more accurate representation of the atmospheric state. Rohrer *et al* (2018) claimed, for instance, that the full-input reanalyses show better agreement within the spectrum of the parameters of anticyclones, cyclones, and circulation types as compared to the surface-input reanalyses. Moreover, a pronounced tendency to underestimate air temperature and precipitation extremes was found in the surface-input reanalyses by Donat *et al* (2016). They highlighted that the time series of climate extreme indices calculated on the basis of those reanalyses are usually 'less extreme' as compared to those obtained from the instrumental observations. Referring to the

extreme weather events, such as floods, hurricanes, and storm surges, also Brönnimann (2017) pointed out that their magnitude is significantly underestimated by the ensemble mean of the 20th Century Reanalysis. The modern, full-input reanalyses resolve the atmospheric state more accurately, however, biases may still exist. As an example, some convective parameters that favour the development of thunderstorms, such as the most unstable convective available potential energy (MUCAPE), are typically overestimated; while the others, such as the mixed layer convective available potential energy (MLCAPE), are underestimated by the full-input ERA-Interim reanalysis (Taszarek *et al* 2018).

Although previous research suggested that climate models and reanalyses may experience difficulties in resolving the state of the lower troposphere under extremely stable atmospheric stratification (e.g. Tjernström and Graversen 2009, Lüpkes *et al* 2010, Medeiros *et al* 2011), a quantitative assessment of their quality in terms of temperature inversions' occurrence is still missing from the scientific literature. Attempts to evaluate the ability of the atmospheric reanalyses to resolve fundamental parameters of the temperature inversions were made by Wetzel and Brümmer (2011) and Zhang *et al* (2011). For instance, Wetzel and Brümmer (2011) found that the frequency of wintertime surface-based inversions over the Arctic is underestimated in the ERA-40 reanalysis as compared to *in-situ* observations. The intra-annual variability of the inversions' depth and strength agrees, in turn, well among the datasets (Wetzel and Brümmer, 2011). Also, the study by Zhang *et al* (2011) confirmed that there is a relatively good agreement between the ERA-Interim reanalysis and upper air soundings in terms of the spatial distribution and seasonal variability of the surface-based temperature inversions over the Arctic and Antarctic. However, some biases in the magnitude of their parameters still occur, e.g. the ERA-Interim reanalysis usually overestimates slightly the frequency of the surface-based inversions. Typically, the uncertainties are smaller in winter and autumn than in summer and spring (Zhang *et al* 2011).

In the previous studies (Palarz *et al* 2018, 2020) we provided a comprehensive climatology of the surface-based and elevated inversions occurring over Europe and the north-eastern Atlantic based on the ERA-Interim reanalysis. We found that the low-tropospheric temperature inversions experience some temporal variability, which is determined mainly by the inversion type. The surface-based inversions exhibit a clear diurnal cycle closely related to the Earth's radiation budget—thus, radiative cooling of the active surface is thought to be the major factor initiating the development of the temperature inversions over Europe (Kassomenos *et al* 2014, Stryhal *et al* 2017). In turn, the day-night variability of the elevated inversions is far less pronounced. They occur most frequently over areas influenced by extensive high-pressure systems—the permanent Azores High and semi-permanent Siberian High, which implies that their development is linked to the large-scale subsidence and adiabatic heating of air parcels (Palarz *et al* 2020). However, an evaluation of the quality of multiple reanalyses under extremely stable atmospheric stratification has not been performed for mid-latitudes yet.

For the first time, we provide here a quantitative assessment of the uncertainties in the parameters of the low-tropospheric temperature inversions among the reanalyses produced by the European Centre for Medium-Range Weather Forecasts (ECMWF) and upper air soundings over Europe. The remainder of the paper is organized as follows: section 2 gives a description of the datasets as well as outlines the methods applied for both identification of the temperature inversions and inter-comparison of their parameters obtained by applying various datasets. In section 3 we provide the results, while discussion and summary are presented in section 4.

2. Data and methods

2.1. ECMWF reanalyses and upper air soundings

This study is based on the newest reanalyses produced by ECMWF, namely ERA-Interim, ERA5, ERA-20C, and CERA-20C, as well as upper air soundings derived from the Integrated Global Radiosonde Archive (IGRA).

The reanalyses utilized here constitute of two categories: (1) the century-long, surface-input reanalyses represented by ERA-20C and CERA-20C as well as (2) the modern, full-input reanalyses represented by ERA-Interim and ERA5 (Fujiwara *et al* 2017, Hersbach *et al* 2018)—detailed information on them are shown in table 1. From all of ECMWF reanalyses, we extracted data of air temperature and geopotential height for the entire vertical cross-section of the troposphere, i.e. from 1000 to 100 hPa, both from the model levels (ModLev) and pressure levels (PresLev). The geopotential values, which are not accessible on ModLev, were computed on the basis of the scripts recommended by ECMWF (2019a) by applying the data on the log of surface pressure and specific humidity. As shown in table 1, both horizontal and vertical resolution of the reanalyses varies greatly among each other. Referring the horizontal resolution, we utilized the data on 0.25° × 0.25°, which is the native resolution of the ERA5 reanalysis. The output resolution was set to 0.25° × 0.25° in the ECMWF data server web interface, which means that the downloaded data were bilinearly interpolated by default. Referring the vertical resolution, in turn, additional computations were performed for the data from PresLev, which, in the lower troposphere, are available at a fixed resolution of 25 hPa.

Table 1. Details on ECMWF reanalyses used in this study. For more information please refer to the paper of Fujiwara *et al* (2017) or to the references contained in table.

Reanalysis	Institution	Available	Model	Horizontal resolution	Vertical levels	Members	Assimilation type	Coupling	References
ERA-Interim	ECMWF	1979–2019	IFS Cycle 31r2	T255	60	1	4D-Var: Full-input	Atmosphere only	Dee *et al* (2011)
ERA5	ECMWF	1979–present	IFS Cycle 41r2	T639	137	10	4D-Var: Full-input	Atmosphere-land	Hersbach, Dee (2016)
ERA-20 C	ECMWF	1900–2010	IFS Cycle 38r1	T159	91	1	4D-Var: Surface-input (surface pressure and marine winds)	Atmosphere only (HadISST2.1.0.0)	Poli *et al* (2016)
CERA-20 C	ECMWF	1901–2010	IFS Cycle 41r2	T159	91	10	4D-Var: Surface input (surface pressure and marine winds)	Atmosphere-ocean (relaxed to HadISST2.1.0.0)	Laloyaux *et al* (2018)

Table 2. List of IGRA upper-air sounding stations considered in this study. Shaded rows indicate stations selected for in-depth analysis of the temperature inversions' parameters.

IGRA station	Latitude	Longitude	Altitude (m AGL)	Observation period	IGRA station	Latitude	Longitude	Altitude (m AGL)	Observation period
Adana	36.98°N	35.35°E	27	1986–2019	Lindenberg	52.22°N	14.12°E	112	1905–2019
Ajaccio	41.92°N	08.79°E	6	1951–2019	Lulea-Kallax	65.54°N	22.11°E	17	1949–2019
Arhangelsk	64.62°N	40.51°E	4	1939–2019	Madrid	40.47°N	03.58°W	631	1950–2019
Athinai-Hellinkon	37.89°N	23.74°E	43	1949–2019	Meiningen	50.56°N	10.38°E	450	1969–2019
Beograd	44.77°N	20.42°E	203	1971–2019	Milano-Linate	45.46°N	09.28°E	104	1949–2019
Bergen	52.82°N	09.92°E	70	1969–2019	Muenchen	48.24°N	11.55°E	484	1976–2019
Bjornoya	74.50°N	19.00°E	20	1957–2019	Murmansk	68.98°N	33.12°E	121	1939–2018
Bodo	67.27°N	14.36°E	11	1942–2014	Nancy	48.68°N	06.22°E	225	1954–2010
Bordeaux-Merignac	44.83°N	00.69°W	51	1920–2019	Nimes-Courbessac	43.86°N	04.41°E	60	1949–2019
Brest-Guipavas	48.44°N	04.41°W	99	1940–2019	Nizhnij Novgorod	56.27°N	44.00°E	161	1946–2019
Brindisi	40.66°N	17.96°E	15	1953–2019	Nottingham	53.01°N	01.25°W	117	1998–2019
Bucaresti-Baneasa	44.51°N	26.08°E	90	1950–2019	Orland	63.71°N	09.61°E	10	1959–2019
Budapest	47.43°N	19.18°E	138	1949–2019	Payerne	46.81°N	06.94°E	490	1943–2019
Cagliari-Elmas	39.24°N	09.06°E	4	1949–2012	Poprad-Ganovce	49.03°N	20.32°E	703	1977–2019
Camborne	50.22°N	5.33°W	87	1949–2019	Praha-Libus	50.01°N	14.45°E	302	1969–2019
Cluj-Napoca	46.78°N	23.57°E	410	1951–2012	Ryazan	54.63°N	39.70°E	155	1962–2019
Ekofisk	56.54°N	03.22°E	52	1994–2019	Samun	41.28°N	36.30°E	4	1952–2019
Emden	53.39°N	07.23°E	0	1952–2011	Sankt Petersburg	59.95°N	30.70°E	72	1946–2018
Gibraltar	36.15°N	5.35°W	3	1951–2015	Schleswig	54.53°N	09.55°E	47	1954–2019
Goteborg	57.66°N	12.29°E	164	1977–2019	Smolensk	54.75°N	32.07°E	240	1939–2019
Greifswald	54.10°N	13.41°E	2	1950–2019	Sondankyla	67.37°N	26.63°E	179	1920–2019
Herstmonceux	50.90°N	00.32°E	52	1993–2019	Stavanger	58.87°N	05.67°E	37	1949–2019
Istanbul-Bolge	40.90°N	29.15°E	18	1951–2019	Stuttgart	48.83°N	09.20°E	314	1957–2019
Izmir	38.43°N	27.17°E	25	1952–2019	Sundsvall-Harnosand	62.53°N	17.44°E	4	1965–2019
Jan Mayen	70.94°N	8.67°W	9	1949–2019	Tallin-Harku	59.40°N	24.60°E	33	1947–2019
Jokioinen Observatory	60.81°N	23.50°E	104	1957–2019	Torshavn	62.02°N	06.76°W	54	1949–2019
Kalach	50.42°N	41.05°E	90	1961–2019	Trappes	48.77°N	02.01°E	167	1949–2019
Kandalasksha	67.17°N	32.35°E	26	1957–2019	Udine	46.03°N	13.18°E	93	1958–2016
Keflavikurflugvollur	63.98°N	22.60°W	52	1946–2019	Valentia	51.94°N	10.24°W	24	1949–2019
Kem	64.95°N	34.65°E	8	1950–2019	Vologda	59.32°N	39.93°E	125	1947–2019
Kharkiv	49.97°N	36.13°E	154	1939–2019	Voronez	51.65°N	39.25°E	100	1939–2019
Kiev	50.40°N	30.57°E	166	1939–2019	Wien	48.25°N	16.36°E	200	1910–2019
Kursk	51.77°N	36.17°E	246	1946–2019	Wroclaw	51.11°N	16.88°E	120	1956–2018
Leba	54.75°N	17.53°E	2	1972–2019	Zadar	44.10°N	15.34°E	78	1982–2019
Legionowo	52.41°N	20.96°E	94	1956–2019	Zagreb	45.82°N	16.03°E	123	1955–2019

Table 3. An example of contingency table for categorical forecasts of a binary event and details on verification measures discussed in this study. For more information please refer to the book of Jolliffe and Stephenson (2003).

Contingency table

		EVENT OBSERVED	
		Yes	No
EVENT FORECAST	Yes	**a** (hit)	**b** (false alarm)
	No	**c** (miss)	**d** (correct rejection)

$n = a + b + c + d$

Verification measure	Definition	Range of values[a]
Proportion Correct (PC)	$PC = \frac{a+d}{a+b+c+d}$	[0, 1]
Probability of Detection (POD)	$POD = \frac{a}{a+c}$	[0, 1]
Probability of False Detection (POFD)	$POFD = \frac{b}{b+d}$	[0, 1]
False Alarm Ratio (FAR)	$FAR = \frac{b}{a+b}$	[0, 1]
Peirce's Skill Score (PSS)	$PSS = \frac{ad-bc}{(b+d)(a+c)}$	[−1, 1]
Heidke Skill Score (HSS)	$HSS = \frac{PC-E}{1-E}$ where E is the proportion of forecasts that would have been correct if forecasts and observations were independent and assuming the same proportion of forecasts of occurrence to non-occurrence, so that for a (2 × 2) contingency table $E = \left(\frac{a+c}{n}\right)\left(\frac{a+b}{n}\right) + \left(\frac{b+d}{n}\right)\left(\frac{c+d}{n}\right)$	[-∞, 1]

[a]Perfect value of each score is indicated as bolded.

The reanalyses provide, access to data at all PresLev, which means that for high-altitude regions, such as the Alps or the Carpathians, they are extrapolated below the surface. Following the recommendation of ECMWF (2019b), we masked out those regions by using the surface geopotential height. Analogous computations were not applied for ModLev—here, the vertical dimensions of ECMWF reanalyses are defined by an eta (η) coordinate, which transitions from purely pressure coordinate at the top and upper levels of the model to a hybrid pressure-sigma coordinate at the mid- to low-levels, and finally to a terrain-following sigma (σ) near the surface (ECMWF, 2018).

As a reference dataset, the upper air soundings derived from the enhanced, version 2 of IGRA were applied. They contain information on air pressure, temperature, geopotential height, relative humidity, dew point depression as well as wind direction and speed at the mandatory levels specified by the World Meteorological Organisation (WMO) and at levels at which a measured variable deviates from linearity. Detailed description of the IGRA dataset as well as information on the quality assurance procedure applied in its production are given by Durre *et al* (2006). Here, we utilized the data from 70 upper-air sounding stations listed in table 2. All of the stations met the criteria of less than 30% missing data in air temperature time series on a monthly basis, which was recommended previously by Guo *et al* (2008). Since the IGRA dataset reports geopotential height (z in meter) only at the mandatory pressure levels, we calculated the thickness of the layer (z_L) between level i of reported geopotential (z_i) and level of unknown geopotential (z_{i+1}) based on the hydrostatic balance formula (Gilson *et al* 2018):

$$\Delta z_L = \frac{R}{g} \cdot \left(\frac{t_i + t_{i+1}}{2}\right) \cdot \ln \frac{p_i}{p_{i+1}},$$

where t_i, t_{i+1} is the air temperature at levels of z_i and z_{i+1} (t in Kelvin), p_i, p_{i+1} is the air pressure at levels of z_i and z_{i+1} (p in hectopascal), R is the ideal gas constant (287 J K^{-1} kg^{-1}), and g is the gravitational acceleration (9.81 m s^{-2}).

Although the overlapping period for ECMWF reanalyses is 1979–2010, we restricted our study to the years 2001–2010 in order to avoid potential inhomogeneity in the time series of the upper-air soundings caused by major changes in sensor types, data correction methods, or station relocation (Gilson *et al* 2018). In addition, keeping in mind the temporal and spatial patterns of the low-tropospheric temperature inversions over Europe discussed by Palarz *et al* (2018) and Palarz *et al* (2020), we examined only the nocturnal temperature inversions occurring in winter (from December to February—DJF) and summer (from June to August—JJA). Usually, the temperature inversions occur most frequently then.

2.2. Methods for the identification of temperature inversions

The tropospheric temperature inversions were identified following the definition of Kahl (1990) and

applied later by among others Wetzel and Brümmer (2011), Zhang *et al* (2011), and Gilson *et al* (2018). The same detection algorithm had been successfully used in our previous studies on the temperature inversions (Palarz *et al* 2018, 2020). Specifically, each of the vertical profiles of air temperature obtained from the reanalyses or upper air soundings was scanned upward to locate the first layer in which air temperature increases with altitude. The inversion base (B) was defined as the bottom of the first layer in which the temperature increases with altitude; whereas the inversion top (T) was defined as the bottom of the first subsequent layer in which the temperature decreases with altitude. The air temperature (t) and geopotential height (z) were then determined at the levels of the inversion base (t_B, z_B) and top (t_T, z_T). By analogy with preceding studies (e.g. Stryhal *et al* 2017, Czarnecka *et al* 2019), we distinguished two types of the temperature inversions: (1) surface-based inversions (SBI) beginning immediately at the lowest level of the reanalyses or upper air soundings and (2) elevated inversions (EI) having bases located at a higher altitude. A quantitative measure of both SBI and EI is given by three parameters, i.e. their frequency ($FQ_{\%}$), depth ($\Delta_z = z_T - z_B$), and strength ($\Delta_t = t_T - t_B$).

Following many previous papers (e.g. Gilson *et al* 2018, Czarnecka *et al* 2019), we restricted our investigation to the temperature inversions whose bases are located up to 3000 m above ground level (AGL), which for low altitudes regions is comparable with the pressure level of 700 hPa. EI depth and strength were calculated solely for the lower-most inversion layer, which is consistent with the studies carried out by Stryhal *et al* (2017), Czarnecka *et al* (2019), and Palarz *et al* (2020). Note also that upper air soundings with fewer than five measurement levels below 700 hPa were discarded from this analysis since we assumed that they may not resolve the vertical structure of the lower troposphere accurately (Kahl *et al* 1992).

2.3. Methods for the inter-comparison of temperature inversions' parameters derived from ECMWF reanalyses and upper air soundings

While a general view on the frequency of SBI and EI is provided on maps created separately for ECMWF reanalyses and upper-air soundings, a more comprehensive comparison of SBI and EI parameters was performed for the ten IGRA upper-air stations indicated in table 2—shaded rows. They have been selected to be representative of various regions over Europe. Following previous study on the relationship between the tropospheric humidity inversions and temperature inversions by Naakka *et al* (2018), *in-situ* observations were compared to the data gained from the grid point closest to each upper-air sounding station.

In order to assess the ability of ECMWF reanalyses to resolve the temperature inversions' parameters, we implemented a variety of deterministic verification measures. Firstly, SBI and EI were regarded as so-called binary events and evaluated utilizing verification measures calculated on the basis of the contingency table—its example and list of the selected measures used in the study are shown in table 3. Secondly, the temperature inversions' depth and strength were evaluated in terms of continuous measures, such as mean systematic error (ME), mean absolute error (MAE), root mean square error (RMSE), and the Pearson's correlation coefficient (ρ). In this paper, we provide Taylor diagrams, in which the degree of correspondence among the various datasets is quantified by three measures, i.e. the Pearson's correlation coefficient, centred root-mean-square error, and standard deviation (Taylor 2001).

3. Results

3.1. Frequency of low-tropospheric temperature inversions

As stated previously, the data from both ModLev and PresLev of ECMWF reanalyses was used for the investigation of the temperature inversions' occurrence. In all reanalyses, some uncertainties among these two data types were found. Surprisingly, their spatial patterns are very similar among the reanalyses although the number of ModLev varies greatly from 60 for the ERA-Interim reanalysis to 137 for the ERA5 reanalysis. As an example, figure 1 illustrates the spatial distribution of the difference in the frequency (FQ_{DIFF}) of the temperature inversions calculated on the basis of the data from ModLev and PresLev for the ERA5 reanalysis. The findings introduced below are, however, relevant for all ECMWF reanalyses. In general, the magnitude of FQ_{DIFF} depends on the inversion type, season, and region. Across mainland Europe, the frequency of summertime SBI identified by applying the data from ModLev is about 30% higher as that obtained by applying data from PresLev. This suggests that a substantial part of summertime SBI is too shallow to be realistically resolved by the data gained from PresLev. Considering wintertime SBI, in turn, FQ_{DIFF} is more spatially heterogeneous. Its magnitude does not exceed 10% over Eastern Europe, where SBI development is usually supported by the large-scale subsidence occurring in the Siberian High. As confirmed by Palarz *et al* (2018), wintertime SBI occurring there are rather deep and strong, thus they can be precisely resolved by the data from both ModLev and PresLev. The difference among the two data types is far more pronounced over the other parts of mainland Europe, in particular over high-altitude regions. Usually, SBI result there from the radiative cooling of the Earth's surface and thus they are rather shallow and weak. On the other hand, the uncertainties identified in EI frequency are slightly smaller and more spatially coherent. The frequency of EI calculated by applying the

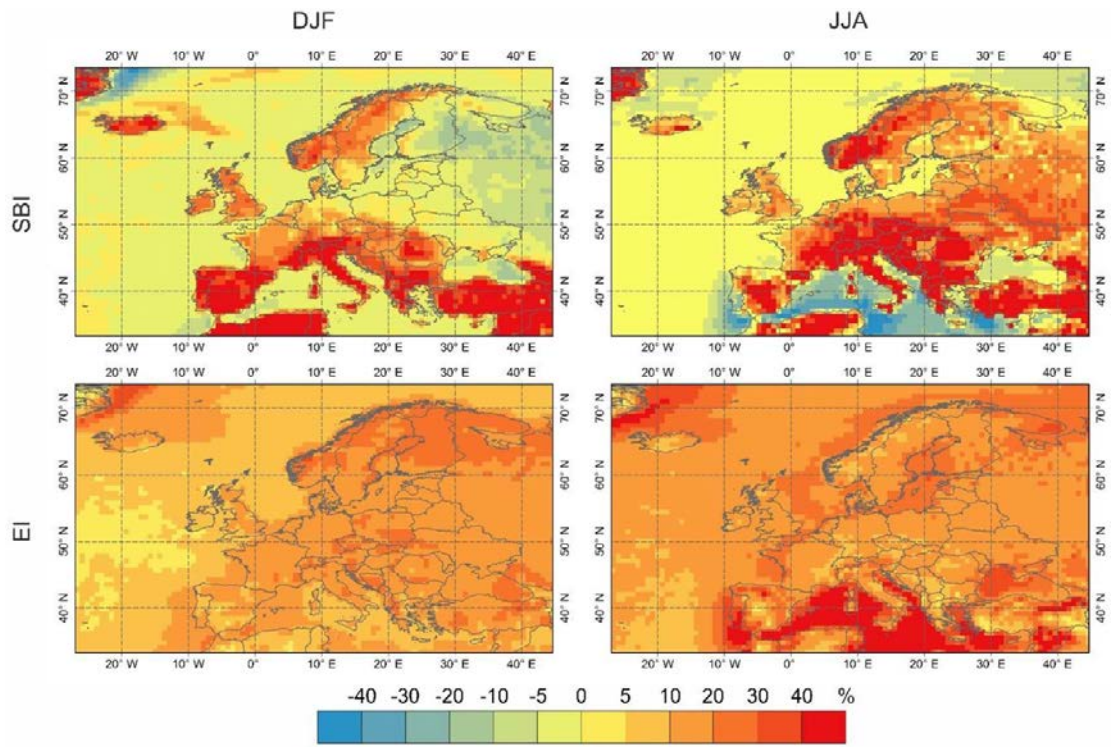

Figure 1. Spatial distribution of the difference in frequency of the low-tropospheric temperature inversions (SBI and EI) calculated based on the data obtained from the model levels (ModLev) and pressure levels (PresLev) ($FQ_{DIFF} = FQ_{ModLev} - FQ_{PresLev}$).

data from ModLev is, however, still positively biased in comparison to data derived from PresLev. Interestingly, over the Mediterranean Sea, the frequency of the summertime temperature inversions calculated based on the data from ModLev is positively biased for EI, while negatively biased for SBI compared to this from PresLev. We hypothesize that this might be a result of incorrect distinction between SBI and EI, however, further research is needed for a detailled analysis of this feature.

A visual inspection of figures 2 and 3 implies that the frequency of both SBI and EI is generally in agreement among ECMWF reanalyses. Typically, SBI are rarely found over marine areas, which is thought to be a consequence of large heat capacity of water providing the possibility of absorbing large amounts of solar energy without significant changes in near-surface air temperature (Palarz *et al* 2018). Across mainland Europe, in turn, SBI reach substantially higher frequency, especially in summer. The frequency of summertime SBI frequency tends to be slightly higher for the ERA-Interim reanalysis as compared to the other reanalyses. Moreover, all ECMWF reanalyses seem to overestimate the frequency of summertime SBI at most of IGRA upper-air stations. In winter, a higher SBI frequency is attained over mountain areas, such as the Alps, the Carpathians, and the Scandinavian Mountains as well as over high altitudes regions of the Iberian Meseta and the Anatolian Plateau. These findings agree well among the reanalyses although, on a more regional scale, some uncertainties are prevalent. The CERA-20C reanalysis, for example, indicates a higher frequency of wintertime SBI over the Scandinavian Mountains as compared to the other ECMWF reanalyses. Similarly to summer, also the frequency of wintertime SBI is overestimated by ECMWF reanalyses at most of IGRA upper-air stations. Slightly larger uncertainties among ECMWF reanalyses are found for EI frequency. They are most pronounced in winter over a marine area west of the Iberian Peninsula and Eastern Europe, which are considered as the two main regions of the most frequent EI occurrence over the domain studied (Palarz *et al* 2020). For both of those areas, the frequency of wintertime EI reach the highest values for the ERA5 reanalysis. Besides, the vast majority of IGRA upper-air stations reports slightly higher EI frequency compared to the reanalyses. The frequency of summertime EI indicates, in turn, a clear distinction between land and marine areas. In all ECMWF reanalyses, EI frequency reaches higher values over the Atlantic Ocean and the Mediterranean Sea, whereas lower values over mainland Europe. Particularly low values of summertime EI frequency are found for the ERA-Interim reanalysis. A visual comparison among the datasets suggests that also summertime EI are underestimated in ECMWF reanalyses, especially over Central and Western Europe.

Further evaluation of the ability of ECMWF reanalyses to resolve the temperature inversions' parameters is performed on the basis of the data

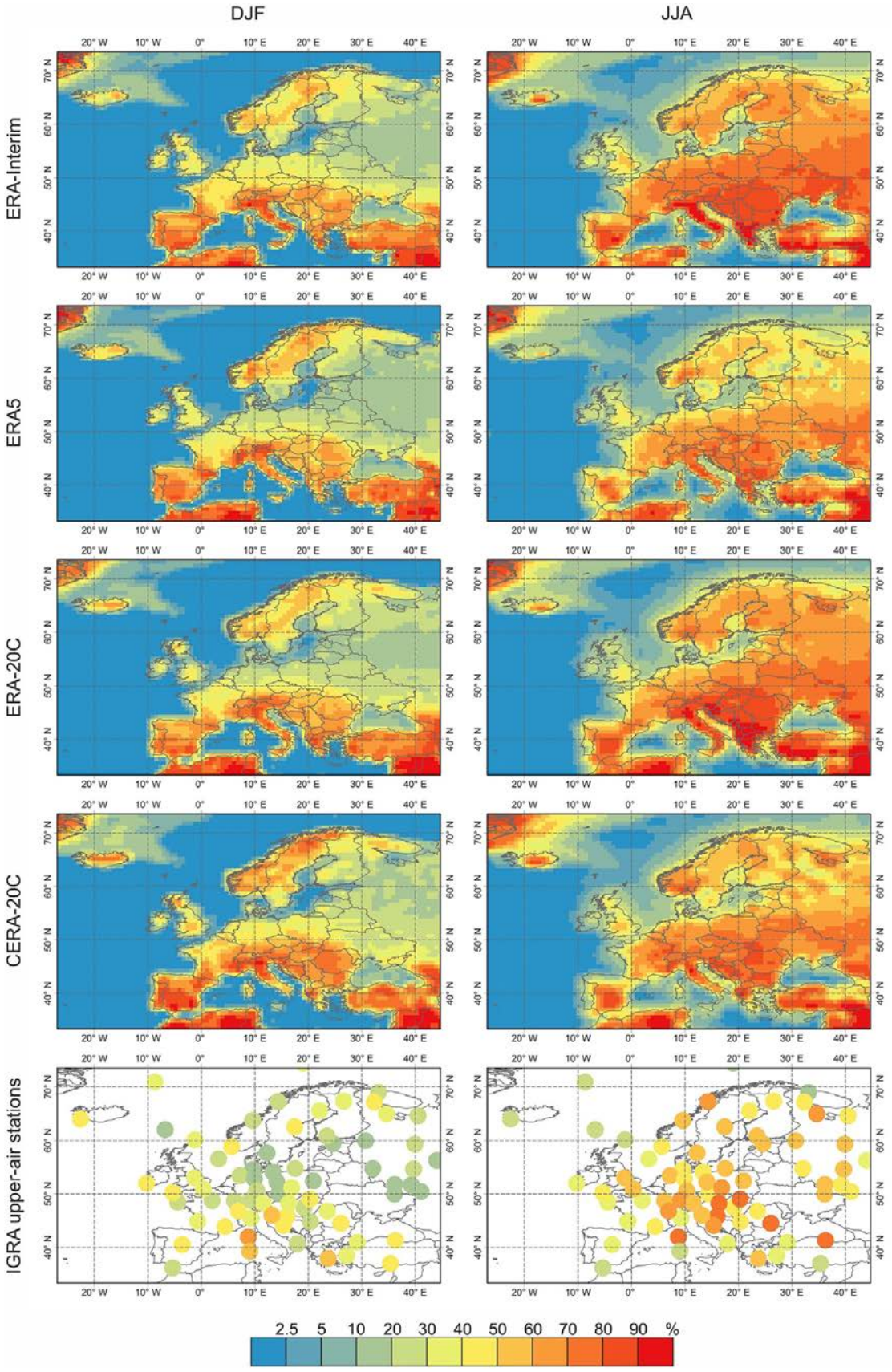

Figure 2. Spatial distribution of seasonal mean frequency of nocturnal SBI calculated separately for winter (DJF) and summer (JJA).

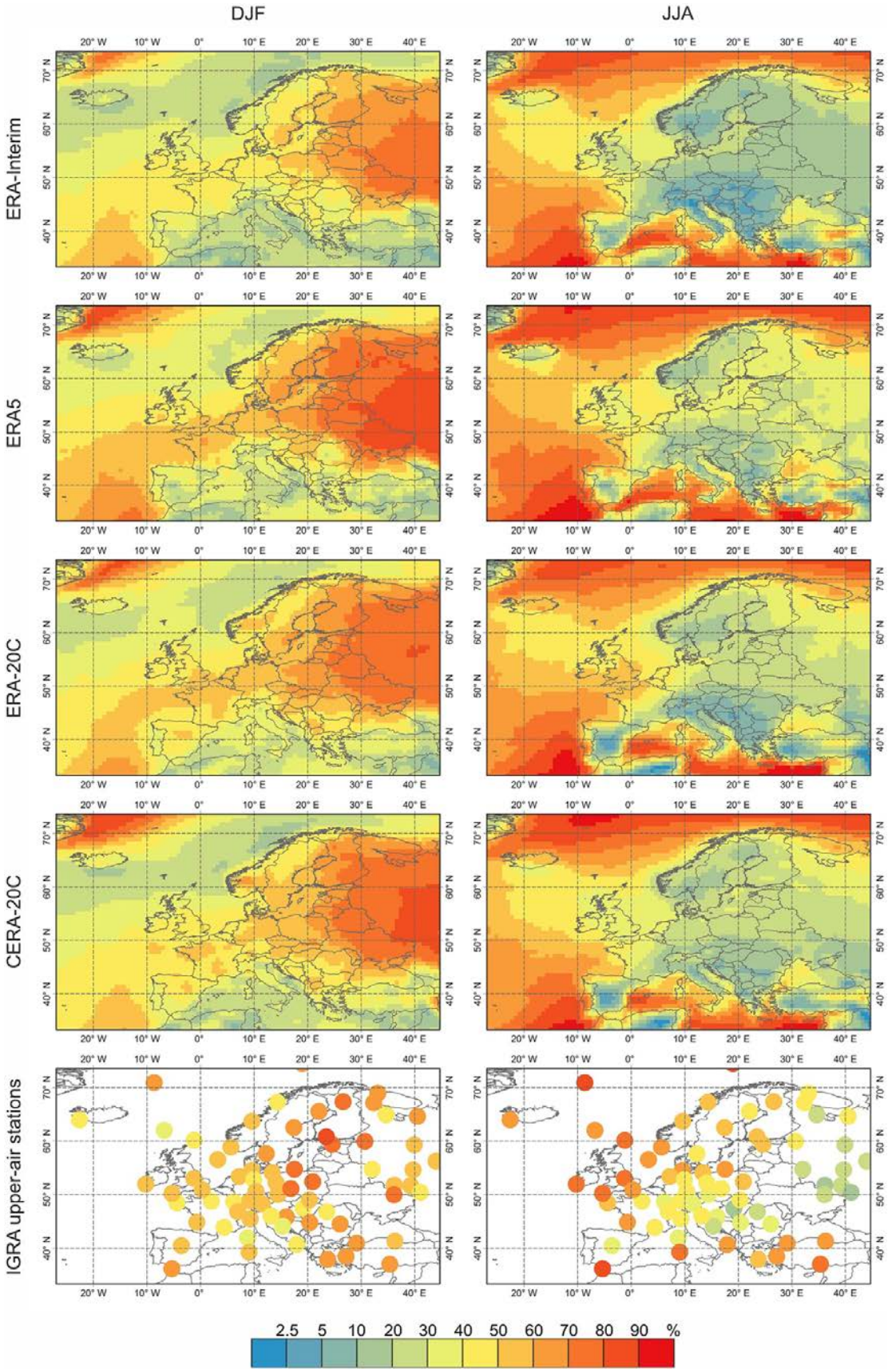

Figure 3. Spatial distribution of seasonal mean frequency of nocturnal EI calculated separately for winter (DJF) and summer (JJA).

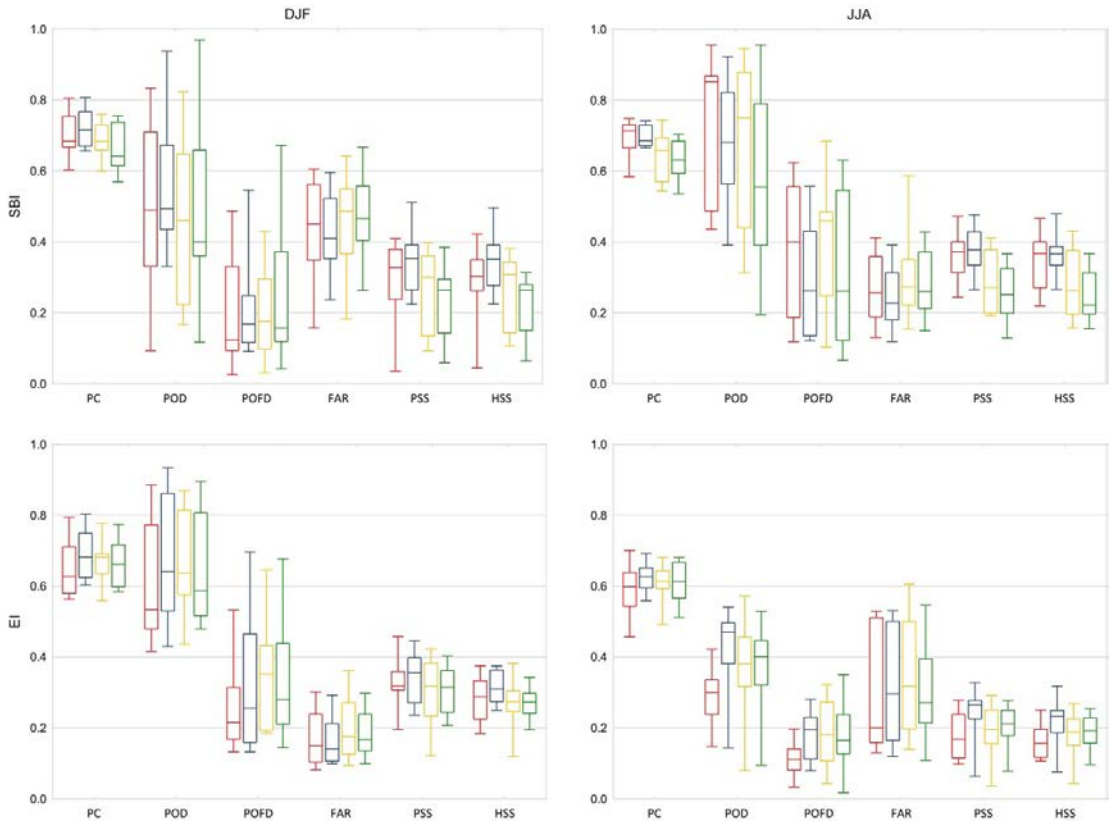

Figure 4. Variability in the values of the deterministic verification measures for ECMWF reanalyses (ERA-Interim—red, ERA5—blue, ERA-20C—yellow, CERA-20C—green) calculated based on the ten IGRA upper-air stations selected. Boxes indicate the interquartile range, whereas whiskers encompass minimum and maximum value of the measure selected. The median is displayed as the central solid line through the boxes.

collected from the ten IGRA stations mentioned before. Figure 4 illustrates the variability in the values of the deterministic verification measures separately for each inversion type and season. Overall, the ability of ECMWF reanalyses to resolve the temperature inversions' occurrence is related to their type, season, and region. Considering large variability in the verification measures, the latter factor is thought to be of high importance here. This variability is particularly large for SBI. Note, however, that over some of the IGRA upper-air stations, the temperature inversions occur very rarely. For such cases, by definition, the application of some verification measures, in particular POD and POFD, may be limited and could give misleading interpretation. As deduced from the FAR values the reanalyses tend to detect SBI, when they actually do not occur, more frequently in winter than in summer. In turn, the values of PC, PSS, and HSS calculated for SBI are characterised by comparable values for both seasons, but some differentiation between the full-input and surface-input reanalyses seems to be visible here–ERA-Interim and ERA5 usually reach slightly higher values as compared to ERA-20C and CERA-20C. In general, the verification measures calculated for EI are much more coherent spatially. Most of them, i.e. PC, POD, FAR, PSS, and HSS, reach values closer to the perfect value for wintertime EI. The values of most verification measures, apart from POFD and FAR, imply that the ERA5 reanalysis tends to detect EI slightly better than the ERA-Interim reanalysis.

3.2. Parameters of low-tropospheric temperature inversions

The degree of correspondence between the depth and strength of the temperature inversions derived from ECMWF reanalyses and IGRA upper-air stations has been quantified using the continuous verification measures. For brevity, we provide here Taylor diagrams that encompass information on the Pearson's correlation coefficient, centred root-mean-square error, and standard deviation (figure 5). The ability of ECMWF reanalyses to resolve the strength of the low-tropospheric temperature inversions strongly depends again on the inversion type, season, and region. Similarly to the verification measures calculated on the basis of the contingency table, also the continuous measures show relatively large spatial variations among the ten IGRA upper-air stations. They are particularly pronounced in winter. Typically, the Pearson's correlation coefficient between ECMWF reanalyses and IGRA upper-air stations is weaker for EI than SBI reaching the lowest values for summertime EI. However, even for SBI, the correlation does not exceed 0.65, which

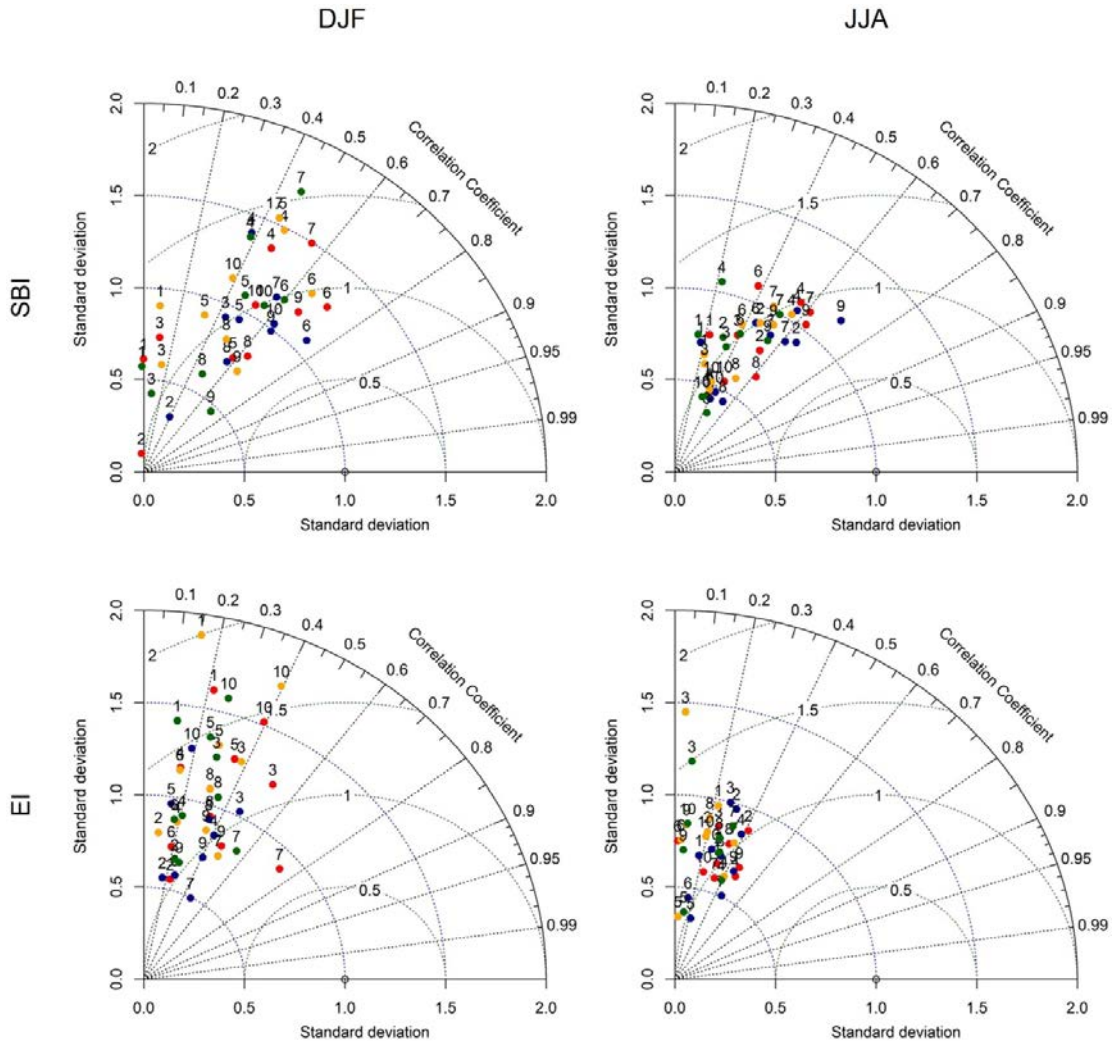

Figure 5. Taylor diagrams displaying a statistical comparison between the temperature inversions' strength obtained from ECMWF reanalyses and IGRA upper-air stations. Colours indicate ECMWF reanalyses (ERA-Interim—red, ERA5— blue, ERA-20 C—yellow, CERA-20 C— green), while numbers represent the ten IGRA upper-air sounding stations selected (1—Bodo, 2—Brindisi, 3—Herstmonceux, 4—Istanbul-Bolgel, 5—Kalach, 6—Madrid, 7—Praha-Libus, 8—Sondankyla, 9—Stavanger, 10—Vologda).

implies that the temperature inversions' strength is rather inaccurately resolved by ECMWF reanalyses. Interestingly, for wintertime SBI and EI, the ERA5 reanalysis presents slightly lower values of standard deviation as compared to the other ECMWF reanalyses suggesting that improvements implemented in physical parametrization schemes and inclusion of more vertical levels may help in better representation of the temperature inversions' strength. Similar conclusions can be drawn for the depth of the temperature inversions (not shown in this paper).

4. Discussion and conclusions

In this study, we have shown that ECMWF reanalyses resolve reasonably well the occurrence of the low-tropospheric temperature inversions over Europe for the period 2001–2010. The quality of their representation is, however, determined by the inversion type, season, and region considered. Over the vast majority of IGRA upper-air soundings stations, SBI frequency is overestimated and EI frequency is underestimated by the reanalyses. Moreover, we found that the ERA-Interim reanalysis, which had been applied in our preceding studies (Palarz *et al* 2018, 2020), experiences the largest differences as compared to the *in-situ* measurements. Our results have demonstrated, however, that the newer reanalyses produced by ECMWF, i.e. ERA5, ERA-20C and CERA-20C, which include improvements in physical parametrization schemes, allow for better representation of the thermal stratification of the lower troposphere. Typically, even the surface-input reanalyses resolve relatively well the main features of the temperature inversions although they assimilate substantially less amount of the input data as compared to the full-input reanalyses.

Larger uncertainties exist, between the frequency of the temperature inversions calculated based on the data from ModLev and that calculated based

on PresLev. Coarser vertical resolution of the data from the PresLev precludes an accurate representation of thin and weak SBI, thus mainly summertime SBI. Conversely, the frequency of EI is reasonably well represented in the data from both ModLev and PresLev, albeit still higher in ModLev. These findings underline that the selection of the data type, namely between the data from ModLev or PresLev, plays an essential role in the outcome of the study and is usually far more important that the selection among multiple reanalyses.

Based on the values of the verification measures, we have shown that the ability of ECMWF reanalyses to detect the low-tropospheric temperature inversions depends on the inversion type, season and region. The latter factor seems to be of high importance here. Particularly regionally-dependent is the detection of SBI, whose development is often shaped by numerous local factors discussed in the preceding papers (e.g. Stryhal *et al* 2017, Gilson *et al* 2018, Palarz *et al* 2018, Czarnecka *et al* 2019). Conversely, EI detection is usually far less related to the micro- and mesoscale factors and thus may be better represented in the reanalyses. The evidence shown in this study indicates also that the ability of ECMWF reanalyses to resolve the temperature inversions' depth and strength is far more limited compared to their frequency. Although ECMWF reanalyses are capable of resolving the general patterns of the depth and strength of the temperature inversions on a seasonal basis, they experience significant uncertainties when considering individual cases of the temperature inversion's occurrence.

Undoubtedly, the upper air-soundings are able to capture finer details of the thermodynamic state of the lower troposphere as compared to the reanalysis products (Bao and Zhang, 2013; Guo *et al* 2016; Nakka *et al*, 2018). Considering, however, the spatial and temporal availability, their application in climate research is often limited. Our study has shown evidence that ECMWF reanalyses provide a fairly accurate representation of the lower troposphere under extremely stable atmospheric stratification and can be utilized in follow-up research. Considering the importance of the atmospheric stratification for climate feedbacks, further investigation of the temperature inversions should focus on their representation in the climate models as well as their long-term variability under the changing climate.

Acknowledgments

A.P. thanks the German Environmental Foundation, *Deutsche Bundesstiftung Umwelt DBU*, for supporting her as a visiting doctoral student at the Justus Liebig University Giessen, Germany through scholarship no. 30018/794, and the National Science Centre, Poland for funding her doctoral studies through the research project ETIUDA no. UMO-2018/28/T/ST10/00425.

Data availability

The data that support the findings of this study are available upon request from the authors.

References

Bao X and Zhang F 2013 Evaluation of NCEP–CFSR, NCEP–NCAR, ERA-Interim, and ERA-40 reanalysis datasets against independent sounding observations over the Tibetan Plateau *J. Clim.* **26** 206–14

Brönnimann S 2017 Weather extremes in an ensemble of historical reanalyses *Historical Weather Extremes in Reanalyses* ed S Brönnimann (*Geographica Bernensia*) 92 7–22

Czarnecka M, Nidzgorska-Lencewicz J and Rawicki K 2019 Temporal structure of thermal inversions in Łeba (Poland) *Theor. Appl. Climatol.* **136** 1–13

Dee D P *et al* 2011 The ERA-Interim reanalysis: configuration and performance of the data assimilation system *Q. J. R. Meteorol. Soc.* **137** 553–97

Donat M G, Alexander L V, Herold N and Dittus A J 2016 Temperature and precipitation extremes in century-long gridded observations, reanalyses, and atmospheric model simulations *J. Geophys. Res.* **121** 3405–20

Durre I, Vose R S and Wuertz D B 2006 Overview of the integrated global radiosonde archive *J. Clim.* **19** 53–68

European Centre for Medium-Range Weather Forecasts (ECMWF) 2018 *IFS Documentation—Cy45r1, Operational Implementation Part II: Data Assimilation* 5 June 2018 (Reading: European Centre for Medium-Range Weather Forecasts)

European Centre for Medium-Range Weather Forecasts (ECMWF) 2019a ERA-Interim: compute geopotential on model levels (https://confluence.ecmwf.int/display/CKB/ERA-Interim%3A\protect$\relax+$compute\protect$\relax+$geopo-\penalty-\@M{}tential\protect$\relax+$on\protect$\relax+$model\protect$\relax+$levels) (Accessed: 30 June 2019)

European Centre for Medium-Range Weather Forecasts (ECMWF) 2019b About pressure level data in high altitudes (https://confluence.ecmwf.int/display/CKB/About\protect$\relax+$pressure\protect$\relax+$level\protect$\relax+$data\protect$\relax+$in\protect$\relax+$high\protect$\relax+$altitudes/) (Accessed: 30 April 2019)

Fujiwara M *et al* 2017 Introduction to the SPARC reanalysis intercomparison project (S-RIP) and overview of the reanalysis systems *Atmos. Chem. Phys.* **17** 1417–52

Gilson G F, Jiskoot H, Cassano J J and Nielsen T R 2018 radiosonde-derived temperature inversions and their association with fog over 37 melt seasons in east greenland *J. Geophys. Res.* **123** 9571–88

Gregow H *et al* 2016 Worldwide survey of awareness and needs concerning reanalyses and respondents views on climate services *Bull. Am. Meteorol. Soc.* **97** 1461–73

Guo J *et al* 2016 The climatology of planetary boundary layer height in China derived from radiosonde and reanalysis data *Atmos. Chem. Phys.* **16** 13309–19

Guo Y, Thorne P W, Mccarthy M P, Titchner H A, Huang B, Zhai P and Ding Y 2008 Radiosonde temperature trends and their uncertainties over eastern China *Int. J. Climatol.* **28** 1269–81

Hersbach H *et al* 2018 Operational global reanalysis: progress, future directions and synergies with NWP. *ERA Report Series* (Reading: European Centre for Medium Range Weather Forecasts) (https://doi.org//10.21957/tkic6g3wm)

Hersbach H and Dee D 2016 ERA5 reanalysis is in production *ECMWF Newsl.* **147** 7–8

Jolliffe I T and Stephenson D B 2003 *Forecast Verification: A Practitioner's Guide in Atmospheric Science* (Chichester: Wiley)

Kahl J D 1990 Characteristics of the low-level temperature inversions along the Alaska Arctic coast *Int. J. Climatol.* **10** 537–48

Kahl J D, Serreze M C and Schnell R C 1992 Tropospheric low-level temperature inversions in the Canadian Arctic *Atmos. Ocean* **30** 511–29

Kassomenos P A, Paschalidou A K, Lykoudis S and Koletsis I 2014 Temperature inversion characteristics in relation to synoptic circulation above Athens, Greece *Environ. Monit. Assess.* **186** 3495–502

Laloyaux P *et al* 2018 CERA-20C: A coupled reanalysis of the Twentieth Century *J. Adv. Modelling Earth Syst.* **10** 1172–95

Lüpkes C, Vihma T, Jakobson E, König-Langlo G and Tetzlaff A 2010 Meteorological observations from ship cruises during summer to the central Arctic: A comparison with reanalysis data *Geophys. Res. Lett.* **37** 1–4

Medeiros B, Deser C, Tomas R A and Kay J E 2011 Arctic inversion strength in climate models *J. Clim.* **24** 4733–40

Naakka T, Nygård T and Vihma T 2018 Arctic humidity inversions: climatology and processes *J. Clim.* **31** 3765–87

Palarz A, Celiński-Mysław D and Ustrnul Z 2018 Temporal and spatial variability of surface-based inversions over Europe based on ERA-Interim reanalysis *Int. J. Climatol.* **38** 158–68

Palarz A, Celiński-Mysław D and Ustrnul Z 2019 Temporal and spatial variability of elevated inversions over Europe based on ERA-Interim reanalysis *Int. J. Climatol.* **40** 1335–47

Poli P *et al* 2016 ERA-20C: an atmospheric reanalysis of the twentieth century *J. Clim.* **29** 4083–97

Rohrer M, Brönnimann S, Martius O, Raible C C, Wild M and Compo G P 2018 Representation of extratropical cyclones, blocking anticyclones, and Alpine circulation types in multiple reanalyses and model simulations *J. Clim.* **31** 3009–31

Stryhal J, Huth R and Sládek I 2017 Climatology of low-level temperature inversions at the Prague-Libuš aerological station *Theor. Appl. Climatol.* **127** 409–20

Taszarek M, Brooks H E, Czernecki B, Szuster P and Fortuniak K 2018 Climatological aspects of convective parameters over Europe: a comparison of ERA-interim and sounding data *J. Clim.* **31** 4281–308

Taylor K E 2001 Summarizing multiple aspects of model performance in a single diagram *J. Geophys. Res.* **106** 7183–92

Tjernström M and Graversen R G 2009 The vertical structure of the lower Arctic troposphere analysed from observations and the ERA-40 reanalysis *Q. J. R. Meteorol. Soc.* **135** 431–43

Wetzel C and Brümmer B 2011 An Arctic inversion climatology based on the European Centre Reanalysis ERA-40 *Meteorol. Z.* **20** 589–600

Zhang Y, Seidel D J, Golaz J C, Deser C and Tomas R A 2011 Climatological characteristics of Arctic and Antarctic surface-based inversion *J. Clim.* **24** 5167–86